



# Discontinuous Galerkin finite element method for solving non-linear model of gradient elution chromatography

Shamsul Qamar<sup>1</sup> · Sadia Perveen<sup>1,2</sup> · Kazil Tabib<sup>1</sup> · Nazia Rehman<sup>1</sup> · Fouzia Rehman<sup>1</sup>

Received: 10 May 2023 / Revised: 3 May 2024 / Accepted: 7 May 2024 / Published online: 20 May 2024  
© The Author(s), under exclusive licence to Springer Science+Business Media, LLC, part of Springer Nature 2024

## Abstract

In this study, a discontinuous Galerkin (DG) finite element method is employed to solve the nonlinear equilibrium dispersive (ED) model, for the simulation of multi-component gradient elution chromatography using a liquid mobile phase in fixed-bed columns. The ED model comprises a set of coupled nonlinear convection-dominated partial differential equations integrated with nonlinear Langmuir type adsorption isotherms. Gradient elution, characterized by the gradual increase in eluent strength through variations in the chemical composition of the mobile phase, is analyzed. An investigation into the advantages of gradient elution chromatography in comparison to isocratic elution is conducted via a sequence of numerical test experiments that assess the influence of solvent strength, modulator concentration, gradient start and end times, and gradient slope on the elution profiles and temporal moments. It has been observed that gradient elution chromatography influences the behavior, shape, and propagation speed of elution profiles, which subsequently affect the cycle time and column efficiency. The results of this study provide significant insights that are critical for understanding, optimizing, and enhancing gradient elution chromatography.

**Keywords** Equilibrium dispersive model · Gradient elution · Langmuir isotherm · Discontinuous Galerkin method · Mass transfer

## Abbreviations

$\alpha$	Solvent strength parameter (–)
$\gamma$	Solvent strength parameter (–)
$\beta$	Gradient slope (–)
$k_{Hr}$	Reference Henry's constant (–)
$b^{\text{ref}}$	Reference non-linearity coefficient (–)
$L$	Column length (–)
$c_{\text{inj}}$	Injected concentration (mol/l)

$t$	Time coordinate (min)
$D_{zr}$	Reference axial dispersion coefficient (cm <sup>2</sup> /min)
$t_e$	Ending time of gradient (min)
$\epsilon$	External porosity (–)
$t_s$	Starting time of gradient (min)
$\phi_0$	Modulator's initial concentration (–)
$t^{\text{inj}}$	Time of injection (min)
$\phi_e$	Modulator's final concentration (–)
$u$	Interstitial velocity (cm/min)
$F$	Phase ratio (–)
$z$	Axial coordinate (–)

✉ Sadia Perveen  
sadia.ahsan@au.edu.pk

Shamsul Qamar  
shamsul.qamar@comsats.edu.pk

Kazil Tabib  
kaziltabib.s@gmail.com

Nazia Rehman  
nazia.asif90@gmail.com

Fouzia Rehman  
fouziarehman838@gmail.com

<sup>1</sup> Department of Mathematics, COMSATS University, Park Road, Chak Shahzad, Islamabad 45550, Pakistan

<sup>2</sup> Department of Mathematics, Air University, PAF Complex, Sector E-9, Islamabad 44230, Pakistan

## 1 Introduction

Chromatographic separation, a fundamental technique for the isolation and purification of substances, utilizes solid stationary and fluid mobile phases. Elution chromatography, specifically, involves the injection of a mixture into an HPLC column to separate its components based on their interactions with the stationary phase. Introduced nearly six decades ago [1], gradient elution has revolutionized analytical liquid chromatography (LC) by continuously varying

the eluent concentration, allowing for the separation of all components in a single run. This is achieved by adjusting the mobile phase composition, often through the addition of a modulator. Despite its extensive use in analytical LC, gradient elution has been less common in preparative LC [2, 3]. However, significant advancements have been made by Snyder et al. [4–8], who have focused on the development of gradient elution techniques for preparative LC, aiming to optimize the separation system. Their work has been supported by both theoretical studies and practical experiments, which have demonstrated the efficiency of gradient elution under ideal conditions for both theoretical and experimental systems.

The efficiency of gradient elution in preparative liquid chromatography was quickly demonstrated in theoretical studies [9, 10] and ideal operating conditions were found for theoretical [11, 12] and experimental separation systems [13]. A discussion on the prediction of retention times in gradient elution mode using isocratic experimental data is given in [14]. The authors in the article [15] discuss the experimental design and re-parameterization of the Neue–Kuss model to enhance the accuracy and precision of predicting isocratic retention factors from gradient measurements in reversed-phase liquid chromatography. The study referenced in [16] showcases the Tecan Freedom EVO, a high-throughput purification tool that enables continuous gradient elution in RoboColumn experiments by delivering liquid more consistently. Jurgen et al. [17] presents a systematic comparison of the elution behavior of plasmid DNA across three widely-used anion exchange resins, employing both linear gradient and isocratic elution experiments. Gradient elution is now commonly used for separating mixtures of components having a broad range of retentivity [18–21]. The method is commonly used in the separation of biopolymers to take advantage of the increased peak capacity that comes with it [22, 23].

Since the beginning of research in this area, there has been a need for an efficient modeling approach for in-depth studies of the technique. This results in highly linear conductivity gradients. Most current gradient elution models are developed for linear concentration ranges. An association between modulator concentrations and component-specific adsorption equilibrium constants is crucial for studying migration processes in the presence of solvent gradients. Until now, linear gradients have been commonly used because they can be defined by simple theoretical relationships [24, 25]. In reversed-phase systems, the LSS model [8, 26, 27] is the most familiar gradient efficient model.

Various difficulties are encountered in the simulation of gradient elution chromatographic systems. Particularly when dealing with nonlinear convection-dominated partial differential equations (PDEs) of chromatographic models incorporating Langmuir isotherms and high column efficiency.

In such scenarios, sharp fronts and narrow peaks can appear in the solutions in a finite time [28, 29]. Because of non-availability of analytical solutions to such model equations, appropriate numerical methods must be applied to ensure stability, efficiency, and physically realistic solutions. A number of numerical techniques are available in the literature, such as Non-Oscillatory Finite Difference methods like total variance diminishing, Essentially Non-Oscillatory (ENO), and Weighted Essentially Non-Oscillatory (WENO) schemes. In contrast, the finite element approaches are capable of dealing with complex boundary conditions and/or geometries. Conventional finite element methods, such as standard Galerkin methods, are unstable and inaccurate for such models and can produce nonphysical solutions. Hughes et al. have proposed the streamline diffusion (SD) process, which subsequently eliminates oscillations based on the numerical solution [30–36]. Nonetheless, hyperbolic PDEs are known to be amenable to explicit solutions, the SD process failed due to its implicit nature in time [37, 38]. Therefore, the discontinuous Galerkin (DG) method was later on introduced to resolve these concerns and to generate stable and high order accurate solutions [33–36]. Reed and Hill proposed this method for solving hyperbolic PDEs [39]. After that, various DG methods for non-linear hyperbolic problems have been formulated. Lesaint and Raviart published the first mathematical study of the method in 1974 [40], demonstrating its applicability to the neutron transport framework. Hulme [41, 42] has proposed an analogous strategy for ODEs just a year before Reed and Hill devised the DG approach, with the exception of the solution approximation being continuous rather than discontinuous. Bassi and Rebay [38] have made significant progress in the study of compressible Navier–Stokes equations using DG space discretization and a new approach for choosing numerical-fluxes. Cockburn and his co-authors have investigated DG methods more deeply in their various articles [43–46]. To prevent numerical oscillations, the DG methods utilize the ideas of slope limiters and numerical fluxes. As these methods are highly parallelizable, they are well suited for complex boundary conditions and complicated geometries.

Numerous differential models exist that characterize the migration of sample zones along chromatographic columns [2]. These models vary in their levels of complexity. The general rate model, acknowledged for its complexity, encompasses all phenomena occurring in the mobile phase, within the pores, and on the stationary phase surface, offering detailed insights into chromatographic processes. In contrast, the simplest ideal model overlooks kinetic processes that cause band broadening, focusing solely on the impact of thermodynamic processes on band profile evolution. Meanwhile, the equilibrium-dispersive (ED) model strikes a balance, proving effective for optimizing chromatographic operations. In most cases of practical interest, the ED model lacks a closed-form analytical

solution, necessitating the use of numerical solutions. Numerous methods exist to compute numerical solutions for the ED Model. The researchers in [47] discuss the development of an orthogonal collocation method that utilizes moving finite elements to simulate fixed-bed adsorbers. This method is based on the Equilibrium Theory for wave transitions and the shock layer theory for shock transitions. A modified approach to the Craig scheme for obtaining a numerical solution of the ED model in gradient chromatography is presented in [48]. Another contribution discussed in [49] is the development and application of the Martin–Synge algorithm for computing the solution of the ED model.

In the present manuscript, the Runge–Kutta discontinuous Galerkin (RKDG) approach is developed to solve the equilibrium dispersive model considering gradient elution. The DG scheme utilizes finite element space discretization in the axial coordinate, which transforms the given PDEs into a system of ODEs. The resultant system is solved by employing a nonlinearly stable explicit high order Runge–Kutta (RK) method that satisfies the total variation bounded property for ensuring the scheme’s positivity. The numerically simulated solutions are used to analyze the impact of gradient starting and ending times, solvent strength, and gradient slope on the profiles of concentration. The obtained results will be useful for understanding and upgrading gradient elution chromatography.

The present article is structured as follows: Sect. 2 provides a discussion on the Equilibrium Dispersive Model (EDM). Section 3 is dedicated to the derivation of the RKDG method within the EDM framework. Numerical case studies are examined in Sect. 4. Finally, Sect. 5 presents the conclusions.

## 2 The EDM for gradient elution

This section aims to introduce the Equilibrium Dispersive Model (EDM) for gradient elution. In the context of gradient elution chromatography, the dynamic behavior of elution profiles is analyzed utilizing the multi-component EDM. This model presupposes that the phase system remains in equilibrium. It is posited that the volume fraction of the non-retained solvent impacts the axial dispersion, Henry’s constants, and the coefficients of nonlinearity. Based on these assumptions, the mass-balance equations for a mixture of  $N_c$  species percolating through the packed-bed column are presented as follows:

$$\frac{\partial c_i}{\partial t} + F \frac{\partial q_i^*(\mathbf{c}, \phi(t, z))}{\partial t} + u \frac{\partial c_i}{\partial z} = \frac{\partial}{\partial z} \left( \left( D_{z,i}(\phi(t, z)) \frac{\partial c_i}{\partial z} \right) \right), \quad i = 1, 2, \dots, N_c. \tag{1}$$

In Eq. 1,  $D_{z,i}$  represents the axial dispersion coefficient for the  $i$ -th component,  $c_i$  denotes the liquid phase concentration of the  $i$ -th component within the mixture,  $\mathbf{c}$  is a vector representing the concentrations of all components,  $u$  is the bulk

interstitial linear velocity, and  $N_c$  signifies the total number of components in the mixture. The variable  $t$  indicates time, while  $z$  refers to the distance along the axial coordinates. Additionally,  $q_i^*$  represents the concentration of non-equilibrium adsorbents for the  $i$ -th constituent. The symbol  $\phi$  indicates the volume fraction of the modified non-retained solvent in gradient elution. Moreover,  $F$  is defined as  $F = \left( \frac{1-\epsilon}{\epsilon} \right)$ , where  $\epsilon$  denotes the total porosity of the system.

The separation of components in a mixture and their migration rates are influenced by their distribution between the mobile and solid phases. In gradient elution, the concentration of a component in the stationary phase,  $q_i^*$ , is influenced by the concentration of the mobile phase modulator, its own local concentration, and the concentrations of all other components. Consequently, the isotherm, which delineates the equilibrium relationship between the concentrations of the  $i$ -th component in the liquid and solid phases, must account for the interdependence of the modulator and the components in sorption behavior. The simplest and most commonly applied model for describing this relationship in a mixture of  $N_c$  components is the Langmuir isotherm, which is formulated as follows:

$$q_i^*(\mathbf{c}, \phi) = \frac{K_{H,i(\phi)} c_i}{1 + \sum_{k=1}^{N_c} b_k(\phi) c_k}, \quad i = 1, 2, \dots, N_c, \tag{2}$$

where

$$K_{H,i}(\phi) = k_{Hr,i} e^{-\alpha\phi}, \quad b_i(\phi) = b_i^{ref} e^{-\alpha\phi}, \quad D_{z,i}(\phi) = D_{zr,i} e^{-\gamma\phi}. \tag{3}$$

The  $i$ -th component reference Henry’s constant is denoted by  $k_{Hr,i}$ . In addition,  $b_i^{ref}$  specifies the degree of nonlinearity inherent in the adsorption isotherm for the  $i$ -th component of the mixture. Here, we aim to obtain the numerical solution for this model in both, linear ( $b_i^{ref} = 0$ ) and nonlinear ( $b_i^{ref} \neq 0$ ) forms. Additionally,  $\alpha$  and  $\gamma$  represent the specific solvent strengths, while  $\phi$  denotes the volume-percent of the modifying non-retained solvent.

For a column which is empty initially, the initial conditions (ICs) are expressed as:

$$c_i(0, z) = 0, \quad q_i(0, z) = 0, \quad i = 1, 2, 3, \dots, N_c. \tag{4}$$

Furthermore, rectangular injections are taken into account in this research. Thus, the boundary conditions (BCs) are stated as:

$$c_i(t, 0) = \begin{cases} c_{i,inj}, & \text{if } 0 \leq t \leq t_{inj}, \\ 0, & t > t_{inj}. \end{cases} \quad i = 1, 2, 3, \dots, N_c. \tag{5}$$

These inlet BCs at the inlet are connected with Neumann BCs at the right end of column

$$\frac{\partial c_i}{\partial z}(t, L) = 0, \quad i = 1, 2, \dots, N_c, \tag{6}$$

where, the concentration of  $i$ -th component concentration in the sample injection is denoted by the symbol  $c_{i,inj}$  and the injection time is represented by  $t_{inj}$ .

The local migration speed of the solute is influenced by the concentration of the mobile phase modulator, represented as  $\phi(t, z)$ , at any given point  $z$  and time  $t$ . The modulator is presumed to be unretained, and band broadening does not alter its profile within the column. As a result, an ideal model can be employed to describe the evolution of  $\phi(t, z)$ . For a column with a length of  $L$ , the preferred model that accounts for changes in the modulator concentration in the liquid phase is outlined as follows:

$$\frac{\partial \phi(t, z)}{\partial t} + u \frac{\partial \phi(t, z)}{\partial z} = 0, \tag{7}$$

with initial and boundary conditions

$$\phi(0, z) = \phi_0, \quad 0 \leq z \leq L, \tag{8}$$

$$\phi(t, 0) = \begin{cases} \phi_0, & \text{if } t < t_s, \\ \Phi(t - t_s), & \text{if } t_s \leq t \leq t_e, \\ \phi_e, & \text{if } t > t_e, \end{cases} \tag{9}$$

where, the starting and ending time are denoted by  $t_s$  and  $t_e$ , respectively. Moreover,  $\phi_0$  and  $\phi_e$  represent the initial and final concentrations of the mobile phase modulator, respectively, and  $\Phi$  denotes the gradient profile that has been implemented. In the case of a linear gradient, the concentration of the modifier at the location  $z$  down the column depends on time and gradient slope which is given as:

$$\Phi(t) = \phi_0 + t\beta, \quad \text{and} \quad \beta = \frac{\phi_e - \phi_0}{t_e - t_s}, \tag{10}$$

where  $\beta$  denotes the slope of the gradient. Elution will be isocratic if  $\beta = 0$ , and will be a negative gradient if  $\phi_0 > \phi_e$ . This article piques our interest in examining the numerical effects of these limited cases as well.

### 3 Derivation of discontinuous Galerkin scheme

In this section, we introduce, formulate, and implement a discontinuous Galerkin (DG) scheme to efficiently solve the nonlinear equilibrium dispersive model used in gradient elution chromatography. The model equations exhibit

profound nonlinearity due to the nonlinear adsorption isotherms. The proposed DG scheme is designed to accurately capture the sharp discontinuities of chromatographic fronts with a minimal number of grid points, thereby reducing computational costs. This scheme offers second-order accuracy both in time and space. It employs a Runge–Kutta DG method along the axial coordinate, transforming the partial differential equations (PDEs) into a system of ordinary differential equations (ODEs). These ODEs are then solved using the Total Variation Bounding (TVB) Runge–Kutta method, which is an explicit nonlinear approach. The essential steps for integrating this numerical algorithm are outlined as follows:

- 1) Across the column’s axial-coordinate, a finite number of grid points divide the computing domain.
- 2) The suggested DG method is applied in axial-coordinate to generate a system of time dependent coupled ODEs.
- 3) The resulting system of ordinary differential equations (ODEs) is approximated using the Total Variation Bounding (TVB) Runge–Kutta method, which is nonlinear and explicit.
- 4) The algorithm is implemented using the C programming language and MATLAB software.

#### 3.1 Implementation of DG-scheme

To implement the discretization of the Discontinuous Galerkin Finite Element (DG-FE) scheme, Eq. 1 is reformulated into two first-order equations. This modification is achieved by rewriting Eq. 1 as follows:

$$\frac{\partial}{\partial t} (c_i + Fq(c_i^*)) + \frac{\partial}{\partial z} \left( uc_i - D_{z,i}(\phi) \frac{\partial c_i}{\partial z} \right) = 0, \quad i = 1, 2, \dots, N_c, \tag{11}$$

and defining the following functions

$$w = w(c_i) := c_i + Fq(c_i^*), \quad g = g(c_i) := \sqrt{D_{z,i}(\phi)} \frac{\partial c_i}{\partial z}, \tag{12}$$

such that

$$f(c_i, g(c_i)) = uc_i - \sqrt{D_{z,i}(\phi)} \left[ \sqrt{D_{z,i}(\phi)} \frac{\partial c_i}{\partial z} \right], \tag{13}$$

$$f(c_i, g(c_i)) = uc_i - \sqrt{D_{z,i}(\phi)} g(c_i). \tag{14}$$

By substituting Eqs. (12)–(14) in Eq. (11), The following PDE system is obtained:

$$\frac{\partial w(c_i)}{\partial t} + \frac{\partial f}{\partial z}(c_i, g(c_i)) = 0, \tag{15}$$

$$g(c_i) = \sqrt{D_{z,i}(\phi)} \frac{\partial c_i}{\partial z}. \tag{16}$$

Before using the proposed numerical technique, the spatial domain along the axial coordinate must be discretized. For simplicity, we will refer to the number of nodes as  $N$ , the discretization index as  $m$ , and the considered computational domain as  $[0, L]$ .  $\Delta z$  and  $z_m$  stand for the width of the mesh intervals and the centres of the cells, respectively, the coordinates  $z_{m-\frac{1}{2}}$  and  $z_{m+\frac{1}{2}}$  are the left and right boundaries of the interval  $\Omega_m \equiv [z_{m-\frac{1}{2}}, z_{m+\frac{1}{2}}]$  for  $1 \leq m \leq N$ , and  $\Omega = \cup \Omega_m$  union of partition of the whole domain.

Let  $w_k(t, z)$  be the approximate numerical solution of  $w(t, z)$  and  $g_k(t, z)$  be the approximate numerical solution of  $g(t, z)$ , such that  $w_k(t, z)$  corresponds to finite-dimensional space for each  $t \in [0, t_{max}]$ . The local solution within each element  $\Omega_m$  is approximated using a polynomial of order  $N$ . We define the approximation space as consisting of piecewise smooth polynomials of order  $N = N_p - 1$ , as follows:

$$U_k = \{ \mu \in L^m(\Omega) : \mu|_{\Omega_m} \in P^p(\Omega_m), \quad \forall \Omega_m \in \Omega, \quad m = 1, 2, 3, 4, \dots, N \}. \tag{17}$$

Where  $P^p(\Omega_m)$  refers to the set of  $p$ -th degree polynomials specified in  $\Omega_m$ . It is worth noting that in  $U_k$ , the functions may have jump discontinuity at the cell interface  $z_{m+\frac{1}{2}}$ . A weak formulation is required to obtain the approximate solution  $w_k(t, z)$ . To obtain weak formulation, multiply Eqs. (15) and (16) by an arbitrary smooth test function  $\mu(z)$ , then integrate by parts over  $\Omega_m$ , [28] we get

$$\int_{\Omega_m} \mu(z) \frac{\partial w(t, z)}{\partial t} dz = - \left( \mu(z_{m+\frac{1}{2}}) f(c_{m+\frac{1}{2}}, g_{m+\frac{1}{2}}) - \mu(z_{m-\frac{1}{2}}) f(c_{m-\frac{1}{2}}, g_{m-\frac{1}{2}}) \right) + \int_{\Omega_m} f(c, g) \frac{\partial u(z)}{\partial z} dz, \tag{18}$$

$$\int_{\Omega_m} \mu(z) g(c) dz = \mu(z) \sqrt{D_{z,i}(\phi)} c(t, z) |_{\Omega_m} - \int_{\Omega_m} \frac{\partial u(z)}{\partial z} \sqrt{D_{z,i}(\phi)} c(t, z) dz. \tag{19}$$

Select  $P_\ell(z)$  Legendre polynomials of order  $\ell$  as the local basis function to execute Eq. (17).  $L^2$ -orthogonality property of Legendre polynomial can be used in this procedure. Generally, orthogonal properties of Legendre polynomials are

$$\int_{-1}^1 P_q(x) P_r(x) dx = \begin{cases} 0, & q \neq r, \\ \frac{2}{2r+1}, & q = r, \end{cases} \quad \text{or} \quad \int_{-1}^1 (P_q(x))^2 dx = \frac{2}{2r+1}, \quad \text{for } q = r. \tag{20}$$

For each  $z \in \Omega_m$  the numerical solution can be written as:

$$w_k(t, z) = \sum_{\ell=0}^p w_m^\ell \varphi_\ell(z), \quad g_k(c_k(t, z)) = \sum_{\ell=0}^p g_m^\ell \varphi_\ell(z), \tag{21}$$

where the polynomial function

$$\varphi_\ell(z) = P_\ell \left( \frac{2(z - z_m)}{\Delta z_m} \right), \quad \ell = 1, 2, 3, \dots, p. \tag{22}$$

If  $p = 0$ , the piecewise constant basis functions are used in the approximate solution  $w_k$ . If  $p = 1$ ,  $w_k$  uses linear basis functions. The linear basis functions are utilized in the current study, and thus  $\ell = 0, 1$ . Furthermore,

$$w_m^\ell(t) = \frac{2\ell + 1}{\Delta z_m} \int_{\Omega_m} w_k(t, z) \varphi_\ell(z) dz, \tag{23}$$

$$g_m^\ell(t) = \frac{2\ell + 1}{\Delta z_m} \int_{\Omega_m} g_k(c_k) \varphi_\ell(z) dz.$$

In this formulation, the exact solutions  $w$  and  $g$  are substituted by their approximate counterparts  $w_k$  and  $g_k$  respectively. Similarly the function  $u(z)$  is replaced by the test function  $\varphi_\ell \in U_K$ . Here  $\{ \varphi_\ell \}_{\ell=1}^{N_p-1}$  serves as a suitable basis for  $U_k$ . Furthermore, at the cell interface  $z_{m+\frac{1}{2}}$ , the function

$f(c_{m+\frac{1}{2}}, g_{m+\frac{1}{2}}) = f(c(t, z_{m+\frac{1}{2}}), g(c_{m+\frac{1}{2}}))$  is not defined. As a result, it must be supplanted by a numerical flux centered on two  $c_k(t, z)$  points at the discontinuity i.e.,

$$f(c_{m+\frac{1}{2}}, g_{m+\frac{1}{2}}) \approx k_{m+\frac{1}{2}} = k(c_{m+\frac{1}{2}}^-, c_{m-\frac{1}{2}}^+). \tag{24}$$

Since  $g := g(c)$ , it can be removed from the arguments of  $k$  for simplification. Then,



$$c_{m+\frac{1}{2}}^- := c_k\left(t, z_{m+\frac{1}{2}}^-\right) = \sum_{\ell=0}^p c_m^\ell \varphi_\ell\left(z_{m+\frac{1}{2}}\right),$$

$$c_{m-\frac{1}{2}}^+ := c_k\left(t, z_{m-\frac{1}{2}}^+\right) = \sum_{\ell=0}^p c_m^\ell \varphi_\ell\left(z_{m-\frac{1}{2}}\right).$$
(25)

The weak formulations in Eqs. (18) and (19) are simplified to:

$$\frac{dw_j^\ell(t)}{dt} = -\frac{2\ell + 1}{\Delta z_m} \left( \varphi_\ell\left(z_{m+\frac{1}{2}}\right) k_{m+\frac{1}{2}} - \varphi_\ell\left(z_{m-\frac{1}{2}}\right) k_{m-\frac{1}{2}} \right) + \frac{2\ell + 1}{\Delta z_m} \int_{\Omega_m} f(c_k, g_k) \frac{d\varphi_\ell(z)}{dz} dz,$$
(26)

$$g_m^\ell(t) = \frac{2\ell + 1}{\Delta z_m} \sqrt{D_{z,i}(\phi)} \left( \varphi_\ell\left(z_{m+\frac{1}{2}}\right) c_{m+\frac{1}{2}} - \varphi_\ell\left(z_{m-\frac{1}{2}}\right) c_{m-\frac{1}{2}} \right) - \frac{2\ell + 1}{\Delta z_m} \sqrt{D_{z,i}(\phi)} \int_{\Omega_m} c_k(t, z) \frac{d\varphi_\ell(z)}{dz} dz.$$
(27)

The liquid concentration  $c$  is required at each time step to update the isotherm function  $q^*(c)$  and flux function  $f(c, g(c))$ . Meanwhile, in each mesh interval  $\Omega_m$ , Eq. (26) gives the modified value of  $w_m = c_m(t) + Fq_m^*(c)$ . To handle this problem, we can use the chain rule and the system of ODE can be achieved in terms of  $c_m$ . Thus, the scheme in Eq. (26) turns out to be

$$\frac{dc_m^\ell(t)}{dt} = -\left[ 1 + \frac{d(F(q^*)_m^{(\ell)}(c))}{dc_m^\ell(t)} \right]^{-1} \left( \frac{2\ell + 1}{\Delta z_m} \right)$$

$$\left( \varphi_\ell\left(z_{m+\frac{1}{2}}\right) k_{m+\frac{1}{2}} - \varphi_\ell\left(z_{m-\frac{1}{2}}\right) k_{m-\frac{1}{2}} \right)$$

$$+ \left[ 1 + \frac{d(F(q^*)_m^{(\ell)}(c))}{dc_m^\ell(t)} \right]^{-1} \left( \frac{2\ell + 1}{\Delta z_m} \right) \int_{\Omega_m} f(c_k, g_k) \frac{d\varphi_\ell(z)}{dz} dz.$$
(28)

Similarly, the scheme in Eq. (27) is of the following form

$$g_m^\ell(t) = \frac{2\ell + 1}{\Delta z_m} \sqrt{D_{z,i}(\phi)} \left( \left( \varphi_\ell\left(z_{m+\frac{1}{2}}\right) c_{m+\frac{1}{2}} - \varphi_\ell\left(z_{m-\frac{1}{2}}\right) c_{m-\frac{1}{2}} \right) \right) - \frac{2\ell + 1}{\Delta z_m} \sqrt{D_{z,i}(\phi)} \left( \int_{\Omega_m} c_k(t, z) \frac{d\varphi_\ell(z)}{dz} dz \right).$$
(29)

The initial data from Eq. (23) for the system described above are as follows:

$$c_m^\ell(0) = \frac{2\ell + 1}{\Delta z_m} \int_{\Omega_m} c(0, z) \varphi_\ell(z) dz, \quad g_m^\ell(0) = g(c_m^\ell(0)).$$
(30)

The choice of appropriate numerical flux is still remaining. The local Lax–Friedrichs flux is utilized in this study because of its simplicity and accuracy:

$$k^{LLF}(a, b) = \frac{1}{2} [h(a, g(a)) + h(b, g(b)) + C(b - a)],$$
(31)

$$\max_{\min(a,b) \leq s \leq \max(a,b)} |h'(s, g(s))|.$$
(32)

The Gauss–Lobatto quadrature method of order 10 is utilized for approximating the integral terms arising in Eqs. (29) & (30).

To avoid numerical oscillations, some restricting methods must be implemented for attaining local monotonicity.

Therefore, it is much necessary to modify  $c_{m+\frac{1}{2}}^\pm$  in the Eq. (24). Then, Eq. (25) can be expressed as

$$c_{m+\frac{1}{2}}^- = c_m^0 + \hat{c}_m, \quad c_{m-\frac{1}{2}}^+ = c_m^0 - \check{c}_m,$$
(33)

where

$$\hat{c}_m = \sum_{\ell=1}^m c_m^\ell \varphi_\ell\left(z_{m+\frac{1}{2}}\right), \quad \check{c}_m = -\sum_{\ell=1}^m c_m^\ell \varphi_\ell\left(z_{m-\frac{1}{2}}\right).$$
(34)

Here, we have taken the linear basis functions such that  $\ell = 1, 0$ . Thus,  $\hat{c}_m$  and  $\check{c}_m$  can be transformed as

$$\hat{c}_m^{(mod)} = mm(\hat{c}_m, \Delta + c_m^{(0)}, \Delta - c_m^{(0)}),$$

$$\check{c}_m^{(mod)} = mm(\check{c}_m, \Delta + c_m^{(0)}, \Delta - c_m^{(0)}),$$
(35)

where  $\Delta^\pm := (c_{m\pm\frac{1}{2}} - c_m)$  and the minmod function is denoted  $mm$ . Equation (33) can be replaced by

$$c_{m+\frac{1}{2}}^{-(mod)} = c_m^{(0)} + \hat{c}_m^{(mod)}, \quad c_{m-\frac{1}{2}}^{+(mod)} = c_m^{(0)} - \check{c}_m^{(mod)}.$$
(36)

Then, Eq. (24) can be modified to

$$k_{m+\frac{1}{2}} = k\left(c_{m+\frac{1}{2}}^{-(mod)}, c_{m-\frac{1}{2}}^{+(mod)}\right).$$
(37)

The accuracy is not affected in those smooth sections and the convergence can be obtained without oscillations in

**Table 1** Reference parameters used in simulations for single-component

Parameters	Values
Column length	$L = 10$ cm
Porosity	$\epsilon = 0.4$
Interstitial velocity	$u = 1.0$ cm/min
Reference Henry’s constant	$k_{Hr} = 5.0$
Reference nonlinearity coefficient	$b^{ref} = 2$
Solvent strength parameter	$\alpha = 0.9$
Reference axial dispersion co-efficient	$D_{zr} = 0.002$ cm <sup>2</sup> /min
Solvent strength parameter	$\gamma = 1.0$
Injected concentration	$c_{inj} = 1$ mol/l
Time of injection	$t_{inj} = 1.0$ min
Modulator’s initial concentration	$\phi_0 = 0.1$
Modulator’s final concentration	$\phi_e = 0.9$
Starting time of gradient	$t_s = 5$ min
Ending time of gradient	$t_e = 80$ min

**Table 2** Reference parameters used in simulations for two-component

Parameters	Values
Reference Henry’s constant	$k_{Hr,1} = 4.5$
Reference Henry’s constant	$k_{Hr,2} = 6.0$
Reference nonlinearity coefficient	$b_1^{ref} = 1$
Reference nonlinearity coefficient	$b_2^{ref} = 2$
Injected concentration	$c_{inj,1} = 1$ mol/l
Injected concentration	$c_{inj,2} = 1$ mol/l

the vicinity of the shock. Ultimately, a Runge–Kutta technique preserving the TVB property is required to solve the obtained ODE-system. On the right end of the column, an outflow boundary condition is used  $c_{N+1}^e = c_N^e$ .

### 4 Numerical case studies

This section outlines some numerical experiments to scrutinize the behaviour of gradient profiles on various key parameters such as  $k_{Hr}$ ,  $\alpha$ ,  $\gamma$ ,  $D_{zr}$  and  $b^{ref}$  characterizing the reference Henry’s constant, the component specific solvent strength parameter, the reference axial dispersion coefficient, and the reference nonlinearity extent coefficient, respectively. In the interest of clarity, the axial dispersion coefficients  $D_{z,i} = D_{zr,i}$ , and the Henry’s constant  $K_{H,i} = k_{Hr,i}$ . At  $z = L$  the solute concentration ( $c$ ) and the modulator concentration  $\phi$  are plotted versus time  $t$ . The concentration profile generated by the DG-FE method is compared to the concentration profile generated by the HR-FVM method. The DG scheme is observed to be more accurate than other flux-limiting FV techniques. In these case studies, the DG scheme enhanced the resolution of the problems. All the required parameters used in the numerical test studies are selected in compliance with commonly used ranges in HPLC applications. The values of optimal parameters occurring in the model equations are catalogued in Tables 1 and 2.

#### 4.1 Elution of single component

Few examples of non linear single component elution are analyzed and presented below:

Figure 1a illustrates the influence of varying Henry’s constant, from  $k_{Hr} = 5$  to  $k_{Hr} = 9$ , using a linear isotherm model, while keeping the solvent strength parameter,  $\alpha$ , fixed at 0.9. The figure highlights changes in peak shapes as  $k_{Hr}$  increases, demonstrating distinct variations in their profiles. In Fig. 1b, the effect of Henry’s constant on the non-linear concentration profiles is explored with a reference value of  $b^{ref} = 2$ . This scenario produces sharp, asymmetrical fronts in the peaks, along with significant differences between

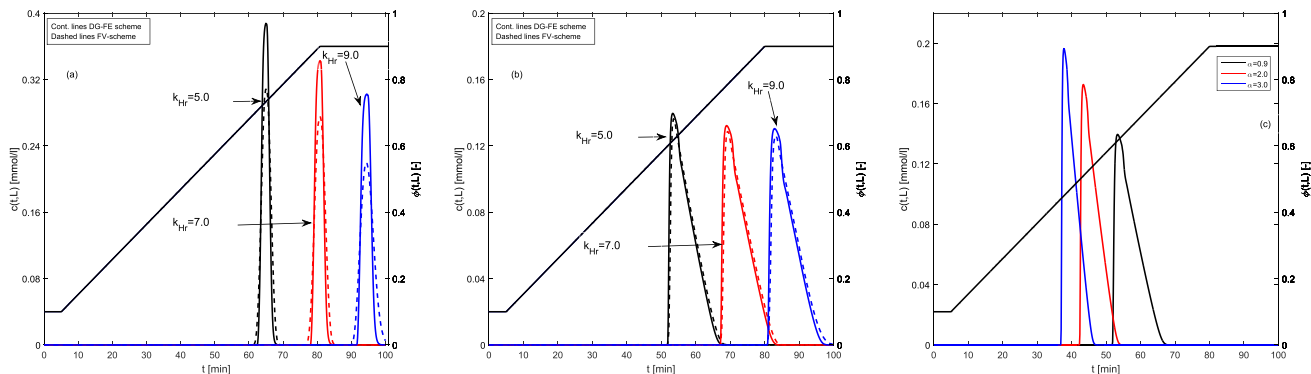


**Fig. 1** Comparison of DG-scheme and FVS for the effects of Henry’s constant  $k_{Hr}$  on **a** linear and **b** nonlinear single-component elution profile. **c** Effects of  $\alpha$  on non-linear single-component elution profile. Other parameters are catalogued in Table 1

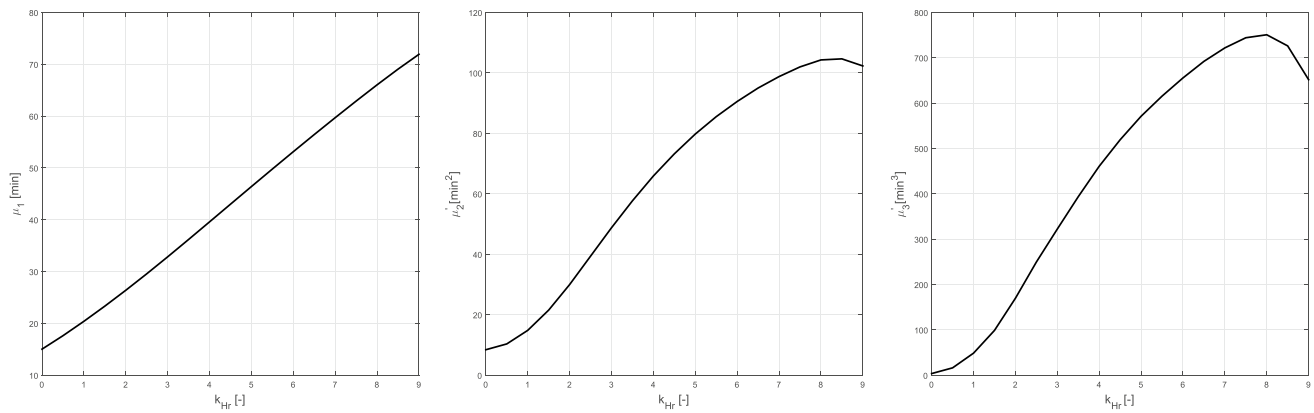


**Fig. 2** Effect of reference Henry's constant  $k_{Hr}$  on temporal moments for  $t_s = 5$  min,  $t_e = 80$  min,  $\phi_0 = 0.1$  and  $\phi_e = 0.95$

them. Additionally, a comparison is made between the Discontinuous Galerkin Finite Element (DG-FE) and Finite Volume (FV) schemes for each value of  $k_{Hr}$ . The results clearly show that the DG method yields more accurate solutions, especially at points of sharp discontinuities, compared to the high-resolution finite volume scheme. Figure 1c examines how variations in the solvent strength parameter,  $\alpha$ , affect the nonlinear single-component elution profile when  $k_{Hr}$  is held constant at 5.0. The findings indicate an increasing sensitivity of the peak profiles to changes in the modulator concentration, influenced by the reference Henry constant.

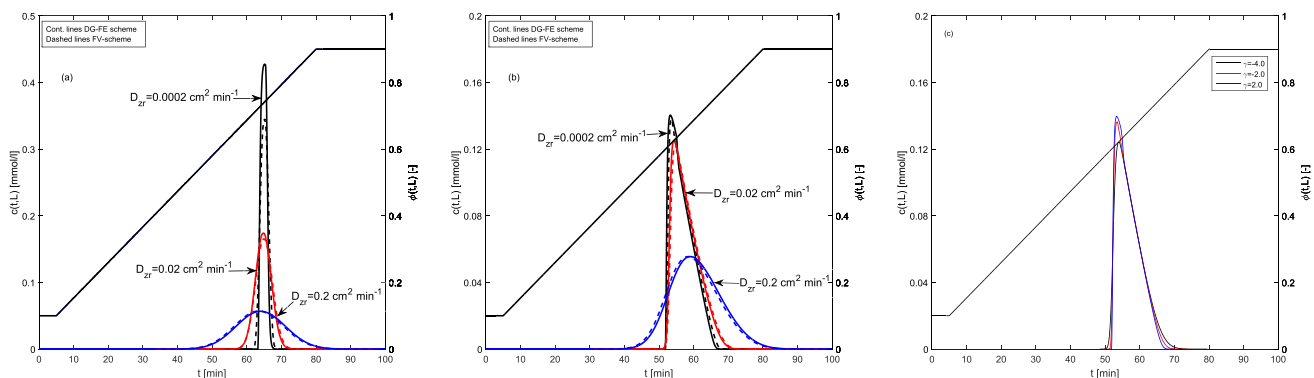
Figure 2 demonstrates how varying Henry's constant,  $k_{Hr}$ , impacts the temporal moments derived from concentration profiles. These moments effectively predict the behavior observed in the concentration profiles. Specifically, the graphs of the first moments show a clear linear relationship, indicating that the mean retention times increase consistently as the Henry constant values rise. Furthermore, when examining higher values of  $k_{Hr}$ , the representations of the second and third central moments reveal noticeable deviations. These deviations highlight more complex dynamics

in peak dispersion and asymmetry, suggesting that higher Henry constants influence not only the retention times but also the spread and shape of the peaks in more pronounced ways.

Figure 3a illustrates the impact of varying the axial dispersion coefficient,  $D_{zr}$ , from 0.1 to 0.0002  $\text{cm}^2/\text{min}$  in a linear isotherm scenario, holding  $\gamma$  at 1.0 and the reference nonlinearity coefficient,  $b^{\text{ref}}$ , at 0. As  $D_{zr}$  decreases, the chromatographic peaks become more sharply defined and narrower, although the retention times at the peak maximum heights remain constant.

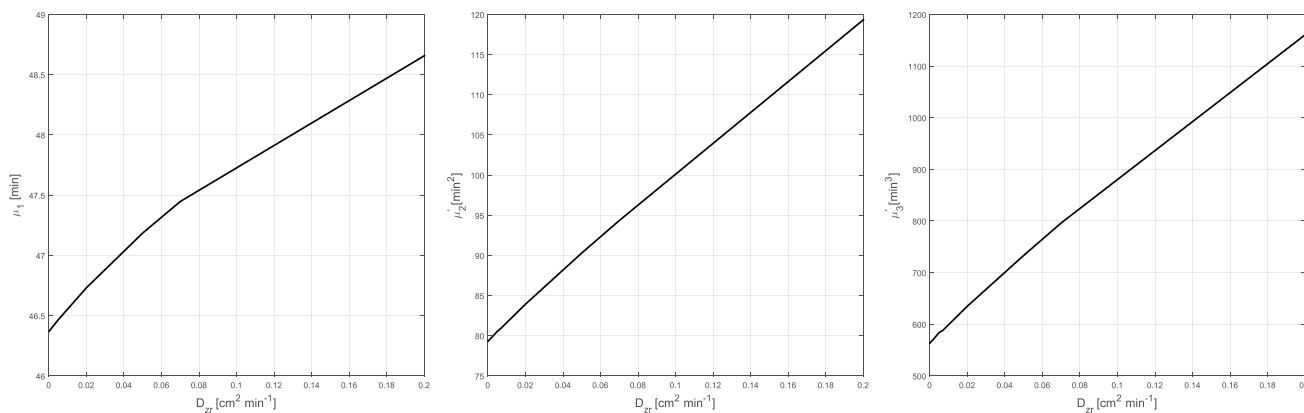
In Fig. 3b, a similar trend is observed under nonlinear isotherm conditions. A comparative analysis between the Discontinuous Galerkin scheme (DG-scheme) and Finite Volume Scheme (FVS) indicates that lower values of  $D_{zr}$  result in steeper, asymmetrical peak fronts. These characteristics are more accurately resolved by the DG-scheme. Notably, in the nonlinear isotherm case, the reduction in  $D_{zr}$  correlates with decreased retention times.

Figure 3c explores the influence of  $\gamma$ , which represents the sensitivity of the axial dispersion coefficient to solvent



**Fig. 3** Comparison of DG-scheme and FVS for the effects of reference axial dispersion coefficient  $D_{zr}$  on **a** linear and **b** nonlinear single-component elution profile. **c** Effects of  $\gamma$  on nonlinear single-component elution profile. Other parameters are catalogued in Table 1





**Fig. 4** Effect of reference axial dispersion coefficient  $D_{zr}$  on temporal moments. Here  $t_s = 5$  min,  $t_e = 80$  min,  $\phi_0 = 0.1$  and  $\phi_e = 0.95$

strength, across a range from  $-4.0$  to  $2.0$ . The findings demonstrate that the responsiveness of the axial dispersion coefficient to variations in solvent strength progressively increases, affecting the nonlinear elution profiles significantly. These results underline the critical role of solvent strength in modulating dispersion within chromatographic systems.

Figure 4 presents the influence of the axial dispersion coefficient,  $D_{zr}$ , on various temporal moments. Analysis of the first moment reveals that an increase in  $D_{zr}$  corresponds to a proportional increase in retention time. This relationship underscores the direct impact of dispersion on solute migration through the chromatographic column.

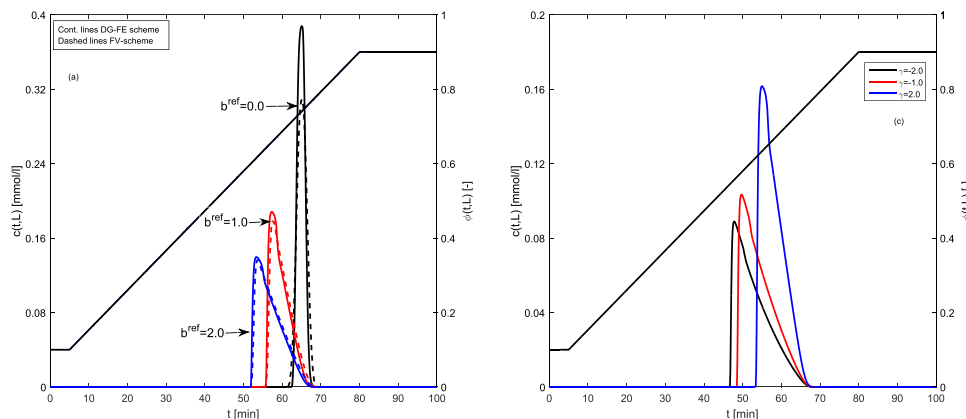
Further examination through the second central moment indicates that the dispersion of the solute profiles broadens as  $D_{zr}$  increases. This broadening effect highlights the enhanced spread of solute distribution within the column due to increased dispersion.

Additionally, the third central moment's plots demonstrate an increase in skewness with rising values of  $D_{zr}$ . This increase suggests that higher dispersion coefficients lead to more pronounced asymmetry in peak shapes.

It is noteworthy that the values derived from these moment calculations align well with those obtained through numerical integration of the elution profiles. This congruence validates the mathematical expressions used for moment calculations and confirms the accuracy of the numerical integration technique in capturing the dynamics of axial dispersion within the chromatographic system.

Figure 5a illustrates the impact of the reference nonlinearity coefficient,  $b^{ref}$ , on the elution profiles, maintaining a constant solvent strength parameter,  $\alpha = 0.9$ . At a coefficient value of  $b^{ref} = 0$ , the elution profile assumes a Gaussian shape. As the value of  $b^{ref}$  increases, the retention time correspondingly decreases, and the elution peaks exhibit increased tailing. The saturation capacity of the stationary phase decreases. This reduction in saturation capacity significantly alters the isotherm shape, which in turn impacts the peak shape observed in chromatographic elution profiles. Additionally, a comparative analysis between the Discontinuous Galerkin (DG) scheme and the high-resolution Finite Volume (HR-FV) scheme is presented as the nonlinearity coefficient varies from 0 to 2. The results indicate that the DG-scheme consistently outperforms the

**Fig. 5 a** Comparison of DG-scheme and FVS of nonlinearity coefficient  $b^{ref}$  on linear single-component elution. **b** Influence of  $\gamma$  on nonlinear single-component elution profile. Other parameters are catalogued in Table 1



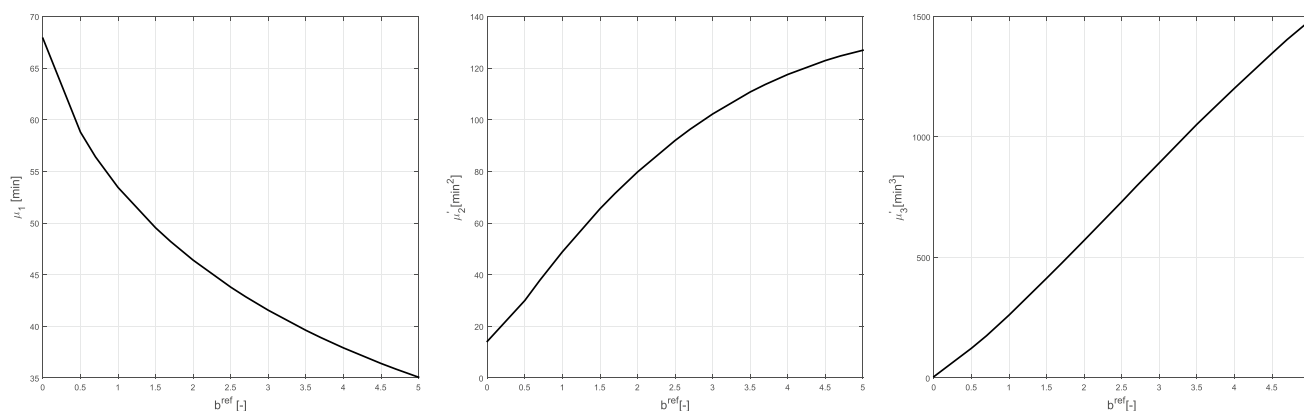
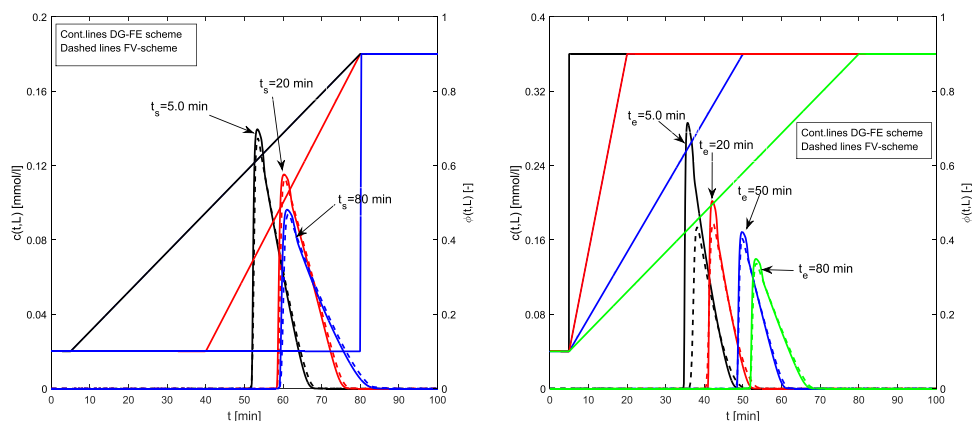


**Fig. 6** Effect of nonlinearity coefficient  $b^{\text{ref}}$  on temporal moments for  $t_s = 5$  min,  $t_e = 80$  min,  $\phi_0 = 0.1$  and  $\phi_e = 0.95$

**Fig. 7** Left plot: Effect of  $t_s$  on elution profiles for  $t_e = 80$  min,  $\phi_0 = 0.1$  and  $\phi_e = 0.95$ . Right plot: Effect of  $t_e$  on elution profiles for  $t_s = 5$  min,  $\phi_0 = 0.1$  and  $\phi_e = 0.95$



HR-FV scheme, especially at points of acute discontinuities, providing more accurate resolutions.

In Fig. 5b, the influence of  $\gamma$  on the nonlinear elution profiles is explored, with  $b^{\text{ref}}$  fixed at 2.0. As  $\gamma$  increases from  $-2.0$  to  $2.0$ , both the peak heights and the retention times of the profiles are observed to increase. This trend highlights the sensitivity of the system's response to changes in  $\gamma$ , affecting the overall dynamics and efficiency of the separation process.

The influence of the nonlinearity coefficient  $b^{\text{ref}}$  on moments is depicted in Fig. 6. The plot of the first moment revealed that the retention time decreases with an increase in the values of  $b^{\text{ref}}$ . The plot of the second moment indicates that the variance of the profiles increases with increments in the  $b^{\text{ref}}$  values. The plot of the third moment depicts that skewness of the fronts significantly improved with higher values of  $b^{\text{ref}}$ . Once again, the values computed directly by moment expressions correlate well with those acquired through numerical integration of the elution profiles.

Figure 7 (left plot) illustrates the effects of varying the gradient start time ( $t_s$ ) while maintaining a constant

gradient end time ( $t_e = 80$  min) on the nonlinear elution profiles. In the case where  $t_s = t_e = 80$  min, a distinct scenario unfolds in which a rapid transition to the isocratic state occurs shortly thereafter, with both initial and final solvent strengths ( $\phi_0$  and  $\phi_e$ ) set at 0.9. Introducing steeper gradients by delaying  $t_s$  leads to broader peaks with reduced heights and extended tails, as well as a deceleration in the chromatographic process. This effect continues until a critical steepness is reached, beyond which the elution is predominantly governed by the initial solvent strength. An inflection point in gradient starting time is observed between 20 and 40 min.

In Fig. 7 (right plot), the impact of the gradient end time ( $t_e$ ) on nonlinear elution profiles is demonstrated. When  $t_s = t_e = 5$  min, there is a swift shift to an isocratic state characterized by  $\phi_0 = 0.1$  and  $\phi_e = 0.9$ . The critical transition point for  $t_e$  is identified to occur between 20 and 30 min. This analysis highlights the significant role of both gradient initiation and termination times in shaping the dynamics of the chromatographic separation process.

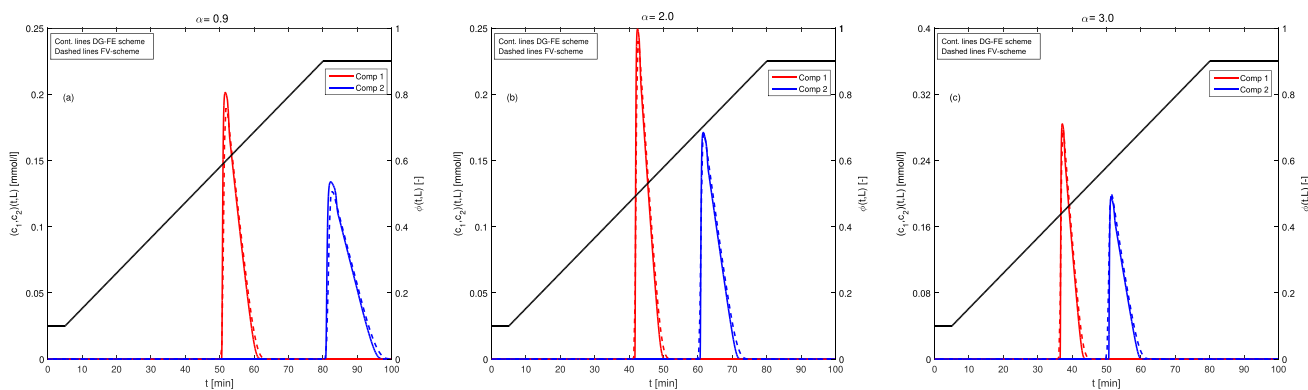


**Fig. 8** Comparison of DG-scheme and FVS for the effects of gradually changing  $\alpha$  on non-linear two-component elution profiles. Other parameters are catalogued in Table 2

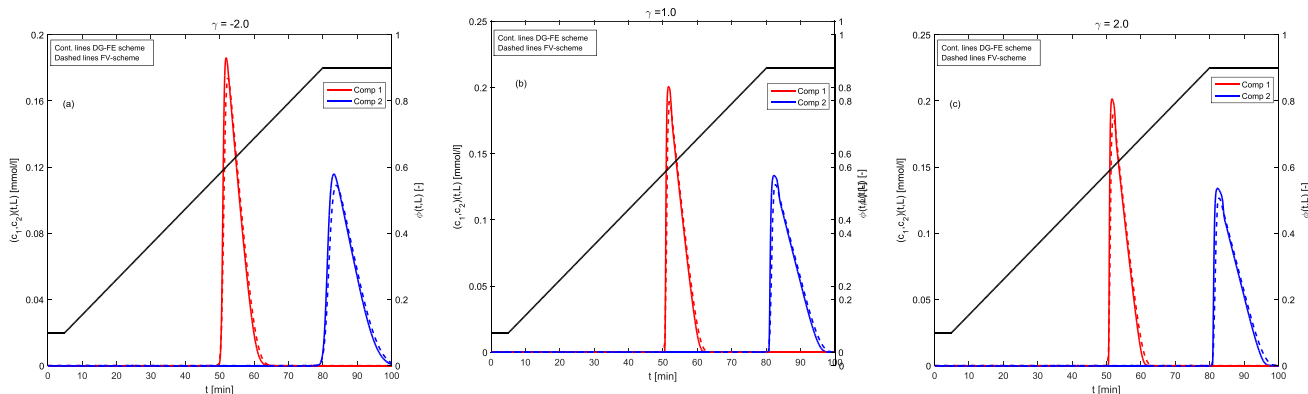


**Fig. 9** Comparison of DG-scheme and FVS for the effects of gradually changing  $\gamma$  on non-linear two-component elution profiles. Other parameters are catalogued in Table 2

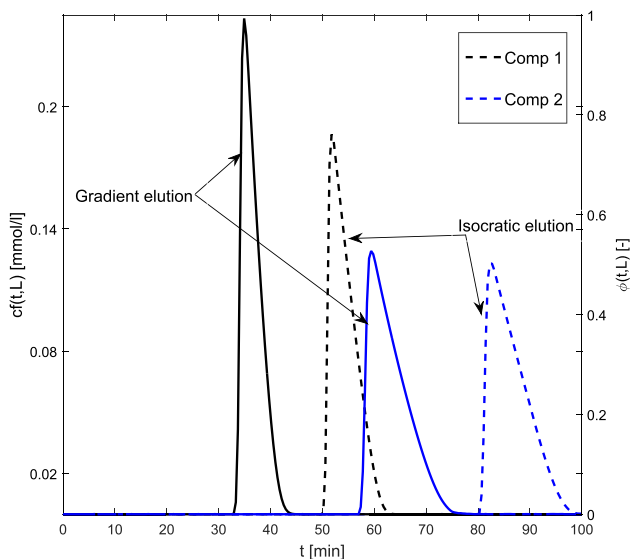


**Fig. 10** Comparison of isocratic and gradient elution considering non-linear isotherms on non-linear two-component elution profile. Other parameters are catalogued in Table 2

### 4.2 Elution of two-component

In Fig. 8a–c, we explore the influence of the solvent strength parameter,  $\alpha$ , on nonlinear elution profiles, where  $\alpha$  ranges from 0.9 to 3.0. The reference Henry constants  $k_{Hr,1} = 4.5$  and  $k_{Hr,2} = 9.0$  remain constant throughout the analysis. As  $\alpha$  increases, there is a noticeable decrease in retention times accompanied by an increase in peak heights for the two components. This pattern indicates that higher solvent strength facilitates faster elution and enhances solute peak prominence.

Conversely, Fig. 9a–c examine the effects of varying  $\gamma$ , the parameter representing the sensitivity of the axial dispersion coefficient to changes in solvent strength, which increases from  $-2.0$  to  $2.0$ . The axial dispersion coefficient is held constant at  $D_{zr} = 0.0002 \text{ cm}^2/\text{min}$ . It is observed that variations in  $\gamma$  do not significantly impact the average retention times of the profiles, suggesting that changes in this parameter primarily affect other aspects of the elution profile, such as peak dispersion and shape, rather than the

overall elution timing. This distinction underscores the different roles that solvent strength and dispersion sensitivity play in the dynamics of chromatographic separation.

Figure 10 presents the outlet profiles of two components under both isocratic and gradient elution conditions, highlighting scenarios where the concentration of modulators varies significantly. The experimental parameters utilized include an axial dispersion coefficient  $D_{zr} = 0.0002 \text{ cm}^2/\text{min}$ , reference nonlinearity coefficients  $b_1^{\text{ref}} = 1.0$  and  $b_2^{\text{ref}} = 2.0$ , Henry constants  $k_{Hr,1} = 4.5$  and  $k_{Hr,2} = 9.0$ , with additional parameters sourced from Table 2.

In isocratic elution, characterized by a constant solvent strength  $\phi_0 = \phi_e$ , the resulting profiles for the nonlinear two-component system are broader, exhibiting significant variances and asymmetries, as well as extended retention times. This outcome suggests a pronounced interaction of the components with the stationary phase under a constant solvent environment, leading to diverse elution dynamics.

Conversely, the profiles obtained from gradient elution are notably more condensed, with reduced retention times. This difference indicates that the varying solvent strength in gradient elution facilitates a more efficient separation process, reducing the interaction time with the stationary phase and leading to sharper, more symmetrical peaks. This comparative analysis underscores the impact of elution mode on the behavior and resolution of chromatographic peaks in multi-component systems.

## 5 Conclusion

The variability of solvent retention activity in gradient elution, influenced by changes in the composition of the mobile phase, renders the mathematical solutions for gradient elution models significantly more complex than those for isocratic elution. This research explored the development and characteristics of elution profiles across various parameters, including modulator concentration, gradient initiation and termination times, gradient slope, and solvent strength. To solve the model equations for both single and dual-component elution, a discontinuous Galerkin (DG-FEM) scheme was employed. This scheme adheres to the Total Variation Bounding (TVB) property and achieves second-order accuracy. Moreover, the scheme offers flexibility for enhancement to higher order accuracies through the incorporation of higher order basis functions and advanced slope limiters, such as Weighted Essentially Non-Oscillatory (WENO) limiters. The efficacy of the DG-scheme was corroborated through comparative analyses with other Finite Volume (FV) schemes documented in the literature. Notably, the DG-scheme demonstrated

superior performance over the high-resolution Koren scheme in numerical test scenarios, particularly in resolving sharp discontinuities and narrow peaks effectively. Gradient elution chromatography is found to be beneficial when there is a significant variation in the retention times of components. In the future, we plan to integrate temperature gradient and solvent gradient techniques to gain further control over the flow rates of analytes within the chromatographic column. This integration will allow us to more precisely manipulate the speed of pulses, enhancing separation efficiency and process optimization.

**Author contributions** Sadia Perveen: conceptualization, methodology, writing, review and editing; Shamsul Qamar: supervision, guidance, review; Kazil Tabib: formal analysis, writing the original draft; Nazia Rehman: validation, writing the original draft; Fouzia Rehman: formal analysis, investigation, methodology.

**Funding** The authors have not received any grants for the current research work from their respective institutions.

**Data availability** The data that support the findings of this study are not openly available due to reasons of sensitivity and are available from the corresponding author upon reasonable request.

## Declarations

**Competing interests** The authors declare that they have no known competing financial interests or personal relationships that could have appeared to influence the work reported in this paper.

**Ethical approval** This declaration is not applicable.

## References

1. Aim, R.S., Williams, R.J.P., Tiselius, A.: Gradient elution analysis. *Acta Chem.* **6**, 826–836 (1952)
2. Guiochon, G., Felinger, A., Shirazi, D.G., Katti, A.M.: *Fundamentals of Preparative and Nonlinear Chromatography*, 2nd edn. Elsevier Academic Press, New York (2006)
3. Miyabe, K., Guiochon, G.: Measurement of the parameters of the mass transfer kinetics in high performance liquid chromatography. *J. Sep. Sci.* **26**, 155–173 (2003)
4. Snyder, L.R.: Linear elution adsorption chromatography: VII. Gradient elution theory. *J. Chromatogr. A* **13**, 415–434 (1964)
5. Snyder, L.R.: Principles of gradient elution. *Chromatogr. Rev.* **7**, 1–51 (1965)
6. Snyder, L.R., Cox, G.B., Antle, P.E.: Preparative separation of peptide and protein samples by high-performance liquid chromatography with gradient elution?: I. The Craig model as a basis for computer simulations. *J. Chromatogr. A* **444**, 303–324 (1988)
7. Cox, G.B., Antle, P.E., Snyder, L.R.: Preparative separation of peptide and protein samples by high-performance liquid chromatography with gradient elution?: II. Experimental examples compared with theory. *J. Chromatogr. A* **444**, 325–344 (1988)
8. Snyder, L.R., Dolan, J.W., Gant, J.R.: Gradient elution in high-performance liquid chromatography?: I. Theoretical basis for reversed-phase systems. *J. Chromatogr.* **165**, 3–30 (1979)

9. Antia, F.D., Horvath, C.: Gradient elution in non-linear preparative liquid chromatography. *J. Chromatogr.* **484**, 1–27 (1989)
10. Tingyue, G., Yung-huoy, T., Gow-jen, T., George, T.: Modelling of gradient elution in multi-component nonlinear chromatography. *Chem. Eng. Sci.* **47**, 253–262 (1992)
11. Felinger, A., Guiochon, G.: Optimizing experimental conditions in overloaded gradient elution chromatography. *Biotechnol. Prog.* **12**, 638–644 (1996)
12. Felinger, A., Guiochon, G.: Comparing the optimum performance of the different modes of preparative liquid chromatography. *J. Chromatogr. A* **796**, 59–74 (1998)
13. Jandera, P., Komers, D., Guiochon, G.: Optimization of the recovery yield and of the production rate in overloaded gradient-elution reversed-phase chromatography. *J. Chromatogr. A* **796**, 115–127 (1998)
14. Tomislav, B., Stefanovic, C.S., Lusa, M., Ukic, S., Rogosic, M.: Development of an ion chromatographic gradient retention model from isocratic elution experiments. *J. Chromatogr. A* **1121**, 228–235 (2006)
15. Sarah, R., Kathryn, C., Dwight, S.: Experimental design and re-parameterization of the Neue-Kuss model for accurate and precise prediction of isocratic retention factors from gradient measurements in reversed phase liquid chromatography (2023). <https://doi.org/10.26434/chemrxiv-2023-zddh7>
16. Kamiyar, R., Andrew, S., Jannat, J., William, R.K., Kevin, S.D., Logan, K., Kelcy, J.N.: Demonstration of continuous gradient elution functionality with automated liquid handling systems for high-throughput purification process development. *J. Chromatogr. A* **1687**, 463658 (2022)
17. Jurgen, B., Matthias, B., Christoph, R., Petra, G., Paul, F.G., Rainer, H.: Desorption of plasmid DNA from anion exchangers: salt concentration at elution is independent of plasmid size and load. *J. Sep. Sci.* **46**(8), 2200943 (2023)
18. Dennis, A., Marek, L., Martin, E., Jörgen, S., Krzysztof, K., Torgny, F.: Fast estimation of adsorption isotherm parameters in gradient elution preparative liquid chromatography, I: the single component case. *J. Chromatogr. A* **1299**, 64–70 (2013)
19. Gritti, F., Guiochon, G.: Separations by gradient elution: why are steep gradient profiles distorted and what is their impact on resolution in reversed-phase liquid chromatography. *J. Chromatogr. A* **1344**, 66–75 (2014)
20. Marek, L., Dennis, A., Martin, E., Jörgen, S., Torgny, F., Krzysztof, K.: Choice of model for estimation of adsorption isotherm parameters in gradient elution preparative liquid chromatography. *Chromatographia* **78**, 1293–1297 (2015)
21. Dennis, D., Marek, L., Tomas, L., Jörgen, S., Krzysztof, K., Torgny, F.: Estimation of nonlinear adsorption isotherms in gradient elution RP-LC of peptides in the presence of an adsorbing additive. *Chromatographia* **80**, 961–966 (2017)
22. Horvath, C., Lipsky, S.: Fast liquid chromatography. Investigation of operating parameters and the separation of nucleotides on pellicular ion exchangers. *Anal. Chem.* **39**, 1422–1428 (1967)
23. Chiara, D.L., Simona, F., Marco, M., Walter, C., Giulio, L., Tatiana, C., Luisa, P., Massimo, M., Alberto, C., Martina, C., Antonio, R.: Modeling the nonlinear behavior of a bioactive peptide in reversed-phase gradient elution chromatography. *J. Chromatogr. A* **1616**, 460789 (2020)
24. Qamar, S., Rehman, N., Carta, S., Seidel-Morgenstern, A.: Analysis of gradient elution chromatography using the transport model. *Chem. Eng. Sci.* **225**, 115809 (2020)
25. Rehman, N., Abid, M., Qamar, S.A.: Numerical approximation of nonlinear and non-equilibrium model of gradient elution chromatography. *J. Liq. Chromatogr. A* **44**(7–8), 382–394 (2021)
26. Jandera, P.: Gradient elution in liquid column chromatography-prediction of retention and optimization of separation. *Adv. Chromatogr.* **43**, 1–108 (2005)
27. Jandera, P., Churacek, J.: Gradient elution in liquid chromatography: I. The influence of the composition of the mobile phase on the capacity ratio (retention volume, band width, and resolution) in isocratic elution-theoretical considerations. *J. Chromatogr.* **91**, 207–221 (1974)
28. Javeed, S., Qamar, S., Ashraf, W., Warnecke, G., Seidel-Morgenstern, A.: Analysis and numerical investigation of two dynamic models for liquid chromatography. *Chem. Eng. Sci.* **90**, 17–31 (2013)
29. Wenda, C., Rajendran, A.: Enantio separation of flurbiprofen on amylose-derived chiral stationary phase by supercritical fluid chromatography. *J. Chromatogr. A* **1216**(50), 8750–8758 (2009)
30. Brooks, A.N., Hughes, T.J.R.: Streamline upwind/Petrov-Galerkin formulations for convection dominated flows with particular emphasis on the incompressible Navier-Stokes equations. *Comput. Methods Appl. Mech. Eng.* **32**, 199–259 (1982)
31. Hughes, T.J.R., Franca, L.P., Mallet, M.: A new finite element formulation for computational fluid dynamics: I. Symmetric forms of the compressible Euler and Navier-Stokes equations and the second law of thermodynamics. *Comput. Methods Appl. Mech. Eng.* **54**, 223–234 (1986)
32. Hughes, T.J.R., Mallet, M., Akira, M.: A new finite element formulation for computational fluid dynamics: II. Beyond SUPG. *Comput. Methods Appl. Mech. Eng.* **54**, 341–355 (1986)
33. Hughes, T.J.R., Mallet, M.: A new finite element formulation for computational fluid dynamics: III. The generalized streamline operator for multidimensional advective-diffusive systems. *Comput. Methods Appl. Mech. Eng.* **58**, 305–328 (1986)
34. Hughes, T.J.R., Mallet, M.: A new finite element formulation for computational fluid dynamics: IV. A discontinuity-capturing operator for multidimensional advective-diffusive systems. *Comput. Methods Appl. Mech. Eng.* **58**, 329–336 (1986)
35. Johnson, C., Saranen, J.: Streamline diffusion methods for the incompressible Euler and Navier-Stokes equations. *Math. Comput.* **47**, 1–18 (1986)
36. Johnson, C., Szepessy, A., Hansbo, P.: On the convergence of shock-capturing streamline diffusion finite element method for hyperbolic conservation laws. *Math. Comput.* **54**(189), 107–129 (1990)
37. Colella, P.: An implicit-explicit hybrid method for Lagrangian hydrodynamics. *J. Comput. Phys.* **63**, 283–310 (1986)
38. Bassi, F., Rebay, S.: An implicit high-order discontinuous Galerkin method for the steady state compressible Navier-Stokes equations. In: Papailiou, K.D., Tsahalis, D., Periaux, J., Hirsh, C., Pandolfi, M. (eds.) *Computational Fluid Dynamics 98*, Proceedings of the Fourth European Computational Fluid Dynamics Conference, vol. 2, pp. 1227–1233. Wiley, Hoboken (1998)
39. Reed, W.H., Hill, T.R.: *Triangular Mesh Methods for the Neutron Transport Equation* (No. LA-UR-73-479; CONF-730414-2), vol. 4, p. 20. Los Alamos Scientific Lab., New Mexico (1973)
40. Lesaint, P., Raviart, P.A.: On a finite element method for solving the neutron transport equation. *Publications Mathematiques et Informatique de Rennes* **S4**, 1–40 (1974)
41. Hulme, B.L.: Discrete Galerkin and related one-step methods for ordinary differential equations. *Math. Comput.* **26**, 881–891 (1972)
42. Hulme, B.L.: One-step piecewise polynomial Galerkin methods for initial value problems. *Math. Comput.* **26**, 415–426 (1989)
43. Cockburn, B., Shu, C.W.: TVB Runge-Kutta local projection discontinuous Galerkin finite element method for conservation laws II. General framework. *Math. Comput.* **52**, 411–435 (1989)
44. Cockburn, B., Hou, S., Shu, C.-W.: TVB Runge-Kutta local projection discontinuous Galerkin finite element method for conservation laws IV: the multidimensional case. *Math. Comput.* **54**, 545–581 (1990)

45. Cockburn, B., Cockburn, C.W.: The Runge-Kutta discontinuous Galerkin finite element method for conservation laws V: multidimensional systems. *J. Comput. Phys.* **141**, 199–224 (1998)
46. Cockburn, B., Shu, C.-W.: Runge-Kutta discontinuous Galerkin methods for convection-dominated problems. *J. Sci. Comput.* **16**, 173–261 (2001)
47. Kaczmarski, K., Mazzotti, M., Storti, G., Morbidelli, M.: Modeling fixed-bed adsorption columns through orthogonal collocations on moving finite elements. *Comput. Chem. Eng.* **21**(6), 641–660 (1997)
48. Kaczmarski, K., Chotkowski, M.: Note of solving equilibrium dispersive model with the Craig scheme for gradient chromatography case. *J. Chromatogr. A* **1629**, 461504 (2020)
49. Horváith, K., Fairchild, J.N., Kaczmarski, K., Guiochon, G.: Martin-Synge algorithm for the solution of equilibrium-dispersive model of liquid chromatography. *J. Chromatogr. A* **1217**(52), 8127–8135 (2010)

**Publisher's Note** Springer Nature remains neutral with regard to jurisdictional claims in published maps and institutional affiliations.

Springer Nature or its licensor (e.g. a society or other partner) holds exclusive rights to this article under a publishing agreement with the author(s) or other rightsholder(s); author self-archiving of the accepted manuscript version of this article is solely governed by the terms of such publishing agreement and applicable law.